Acta Geodyn. Geomater., Vol. 20, No. 2 (210), 49–60, 2023
DOI: 10.13168/AGG.2023.0005
journal homepage: https://www.irsm.cas.cz/acta

ORIGINAL PAPER

A DECORRELATION FILTER BASED ON THE FULL ERROR COVARIANCE OF GRACE GRAVITY FIELD SOLUTIONS

Xiaolei JU [1)], Yunzhong SHEN [2)] and Qiujie CHEN [2), *]

[1)] *School of Civil Engineering, Shandong Jiaotong University, 5001 Haitang Road, Jinan Shandong 250357, China;*
[2)] *College of Surveying and Geo-Informatics, Tongji University, Shanghai 200092, China*

**Corresponding author's e-mail:* chenqiujie2009@163.com

ARTICLE INFO

Article history:
Received 6 November 2022
Accepted 12 June 2023
Available online 27 June 2023

Keywords:
Time variable gravity field
GRACE
Noise-reduction filter
Mass change

ABSTRACT

We propose a decorrelation filter (noise-reduction filter) constructed by using the full error covariance matrix information of the spherical harmonic solutions derived from the observations of the Gravity Recovery and Climate Experiment (GRACE) mission. To construct the noise-reduction filter, the filter factors are inversely proportional to the eigenvalues of the covariance matrix. Using the designed noise-reduction filter, we can significantly reduce the north-south stripes in monthly GRACE gravity field solutions. Our study shows that the noise-reduction filter can achieve higher signal-to-noise ratio as compared to other filtering methods under consideration, i.e., P_3M_8 and P_4M_6 as well as Gaussian smoothing. Using the noise-reduction filter, the estimated mass rates over the entire Antarctica, East Antarctica and West Antarctica (including the Antarctica Peninsula) are -107.38±41.06 Gt/yr, 36.42±14.40 Gt/yr and -147.45±16.78 Gt/yr respectively, consistent with the results from the P_3M_8 filter and P_4M_6 combined with Gaussian filter.

1. INTRODUCTION

The twin-satellite mission of the Gravity Recovery and Climate Experiment (GRACE) was launched in March 2002 and stopped operation in October 2017 (Tapley et al., 2004). With over 15 years of GRACE observations, the monthly gravity solutions have been widely used to analyze the global mass changes with about 400 km resolution (Tapley et al., 2004) and about 1-cm equivalent water height (Wahr et al., 2004), especially over the Antarctic Ice Sheet (AIS) (Shum et al., 2008; Velicogna et al., 2013; Velicogna et al., 2014; Ju et al., 2014; Chen et al., 2009; Loomis et al., 2020; Zou et al., 2019; Gao et al., 2019).

Due to the instrument errors and polar orbital configuration, there exist obvious north-south stripes in the GRACE time-variable gravity field models. Such stripe errors are successfully eliminated or decreased via some filtering methods, including the Gaussian filter (Jekeli, 1981; Sasgen et al., 2016; Chen et al., 2006; Zhang et al., 2009; Han et al., 2005), the decorrelation and approximately decorrelating filter technique (Chambers, 2006; Swenson and Wahr, 2006; Chen et al., 2008; Duan et al., 2009), the Empirical Orthogonal Functions (EOF) filter (Rangelova et al., 2007; Wouters and Schrama, 2007), the Singular Spectrum Analysis (SSA) (Wang et al., 2011) and the Multichannel Singular Spectrum Analysis (MSSA) (Zotov and Shum, 2010; Guo et al., 2018; Prevost et al., 2019; Wang et al., 2020), the Slepian method (Simons et al., 2006) and the wavelet analysis (Panet et al., 2007; Fengler et al., 2007), as well as the regularization method by using the prior error information of the gravity field model (Kusche, 2007). Kusche et al. (2009) proposed the DDK filter that using no signal covariances in the spherical harmonics (SH) domain, which propagates to a full covariance matrix in the spatial domain. This DDK filter can be downloaded from the website ICGEM (http://icgem.gfz-potsdam.de/ICGEM/). Klees et al. (2008) developed the filtering method using signal variances but no covariances in the spatial domain and propagated them to the full matrix in the SH domain (Klees et al., 2008). Davis (2008) designed a filter in the spatial domain, which has similar properties with the Gaussian smoothing (Davis, 2008). When constructing the filtering matrix, the two methods (Kusche, 2007; Kless et al., 2008) need not only the covariance matrix of the GRACE solution but also a priori covariance information of the spatial domain signal. However, using the prior covariance of the signal is essentially a constraint solution, and unreasonable prior information can distort the mass change signal. Thereby, we try to develop a noise-reduction filter by only using the error covariance matrix of the GRACE solutions.

Cite this article as: Ju X, Shen Y, Chen Q: A decorrelation filter based on the full error covariance of GRACE gravity field solutions. Acta Geodyn. Geomater., 19, No. 2 (210), 49–60, 2023. DOI: 10.13168/AGG.2023.0005

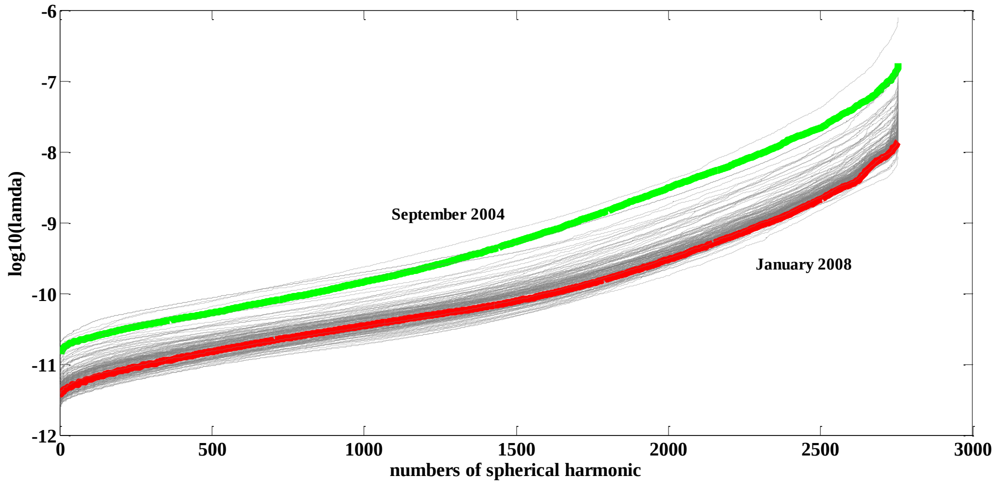

Fig. 1 The eigenvalues of the error covariance matrices (green-February 2004, red-January 2008, the remaining 153 months are gray, Y label is using a logarithmic scale).

The rest of this paper is organized as follows. In Section 2, the noise-reduction filter is developed based on the error covariance matrix of GRACE spherical harmonic solutions. In Section 3, the effectiveness of the noise-reduction filter is demonstrated by comparing the noise-reduction filter to the traditional P_nM_m decorrelation filter (Swenson and Wahr, 2006; Chen et al., 2008). In Section 4, the temporal and spatial characteristics of AIS mass changes are analyzed. The discussion and conclusions are given in Sections 5 and 6 respectively.

2. NOISE-REDUCTION FILTER METHOD

Since the GRACE Spherical Harmonic (SH) coefficients up to degree and order 8 are dominated by signals (Swenson and Wahr, 2006), the noise-reduction filter is designed to filter the SH coefficients beyond degree and order 8. The GRACE SH coefficients are truncated to degree and order 60 and the effects of atmosphere, ocean and tides have been removed from estimating the SH coefficients (Bettadpur, 2012). When solving for the GRACE SH coefficients, the corresponding covariance matrix is also computed and used to evaluate the formal errors of the estimated SH coefficients. The covariance matrix Q can be orthogonally decomposed as,

$$Q = P\Lambda P^T \tag{1}$$

where Λ is a diagonal matrix sorted in ascending order with k-th diagonal element λ_t, and P are the eigenvectors. The eigenvalues of the error covariance matrices of all months are shown in Figure 1 for Tongji-GRACE2018 models (Chen et al., 2019). In Figure 1, the eigenvalues of September 2004 and January 2008 are presented in green and red respectively, while the eigenvalues of the remaining 153 months are shown in gray. The solution of September 2004 suffers from a short repeat orbit (with bad condition) (Chen et al., 2019) and that of January 2008 is in the middle of the GRACE period (with good condition). Here we need to point out that the orbital altitude of GRACE became very low at the end of GRACE lifetime. As we know, the decreased orbital altitude is more sensitive to the gravity field signals at high degrees and orders, leading to improved accuracy of geopotential coefficients at high degrees and orders.

Furthermore, the formal errors of the unconstrained gravity field solutions for the months September 2004 and January 2008 are both presented in the form of order and the degree in Figure 2. It indicates that the noise of the unconstrained solutions increases with degree and order.

The SH coefficients are usually expressed as $\{C_{lm}, S_{lm}\}$, where l and m denote the degree and order. After removing the average SH coefficients of all months $\{\bar{C}_{lm}, \bar{S}_{lm}\}$, the differences of SH coefficients $\{\Delta C_{lm}, \Delta S_{lm}\}_i$ month are expressed as,

$$U = \{\cdots, \Delta C_{lm}, \Delta S_{lm}, \cdots\} \tag{2}$$

Using the decomposed orthogonal matrix P in Eq. (1), we can transform the SH coefficients U to the uncorrelated coefficients R with,

$$R = P^T U \tag{3}$$

Obviously, the error covariance matrix of the transformed coefficients R is just the diagonal matrix Λ. Since large noise exists in the SH coefficients of high degrees, a reasonable filter is to suppress the noise at high degrees and keep the signals at low degrees. In other words, the higher the degree SH coefficients are, the smaller the filter factors should be applied to. While for the coefficients which are dominated by signals, the corresponding filter factors should be close to 1 to avoid signal loss. For GRACE SH coefficients, the first 8 degrees and orders are not filtered since the coefficients are dominated by signals (Swenson and Wahr, 2006). Because the error covariance matrix can reflect the actual noise of the

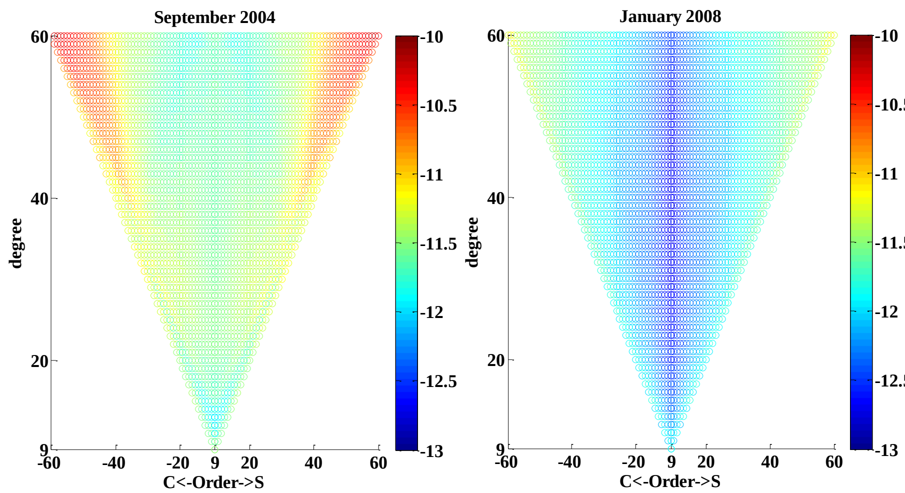

Fig. 2 The formal errors of unconstrained solutions (Y label is using a logarithmic scale) in September 2004 and January 2008.

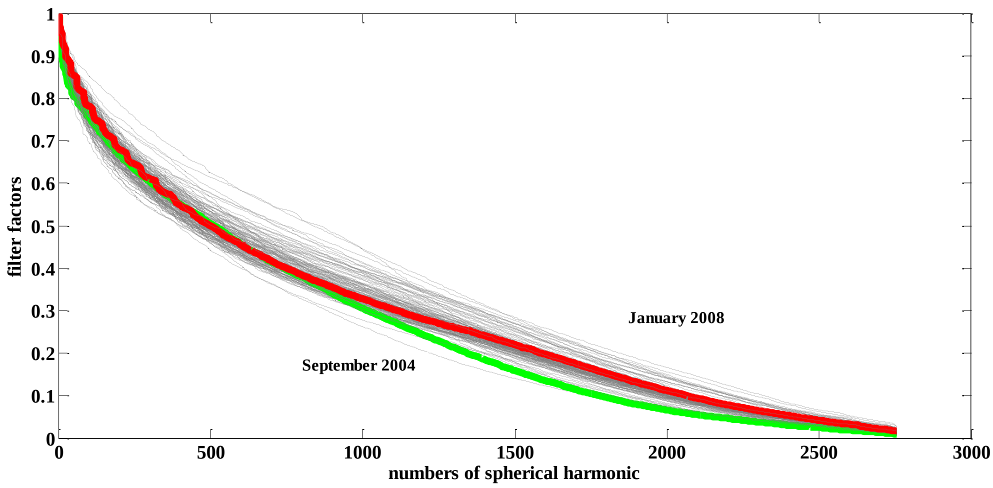

Fig. 3 The distribution of noise-reduction filter factors (green-September 2004, red-January 2008, the remaining 153 months are marked in gray).

SH coefficients, designing a filter function based on the full covariance matrix is reasonable and necessary. Since the transformed SH coefficients R with Eq. (3) are uncorrelated, the diagonal matrix Λ just indicates the covariance matrix of the coefficients R. Thus, the filter factors are designed as $F = \sqrt{\lambda_1}\sqrt{\Lambda^{-1}}$, the filtered transformed SH coefficients R_{filter} are,

$$R_{filter} = \sqrt{\lambda_1}\sqrt{\Lambda^{-1}}R \tag{4}$$

where λ_1 is the first eigenvalue of the error covariance matrix of the SH coefficients, after the first 8 degrees and orders are removed. The final SH coefficients U_{filter} can be expressed as,

$$U_{filter} = PR_{filter} \tag{5}$$

By substituting Eq. (3) into Eq. (4) and then into Eq. (5), we have

$$U_{filter} = P\sqrt{\lambda_1}\sqrt{\Lambda^{-1}}P^T U = F'U \tag{6}$$

where the filter factors $F' = P\sqrt{\lambda_1}\sqrt{\Lambda^{-1}}P^T$ are symmetric matrixes directly applied to the original SH coefficients U.

Figure 3 demonstrates the characteristics of the designed filter factors F, which decrease with degree and order. Since there are so many months concentrated together that we cannot clearly identify the two highlighted months (i.e., September 2004 and January 2008), an additional sub-figure is provided at the top-right corner of Figure 3. The noise of the SH coefficients at higher degrees and orders is gradually suppressed, while the signals at lower degrees and orders are mostly retained. The solutions of September 2004 and January 2008 are considered as a bad and a good one respectively. The corresponding filter factor of the former is smaller, especially at high degrees and orders.

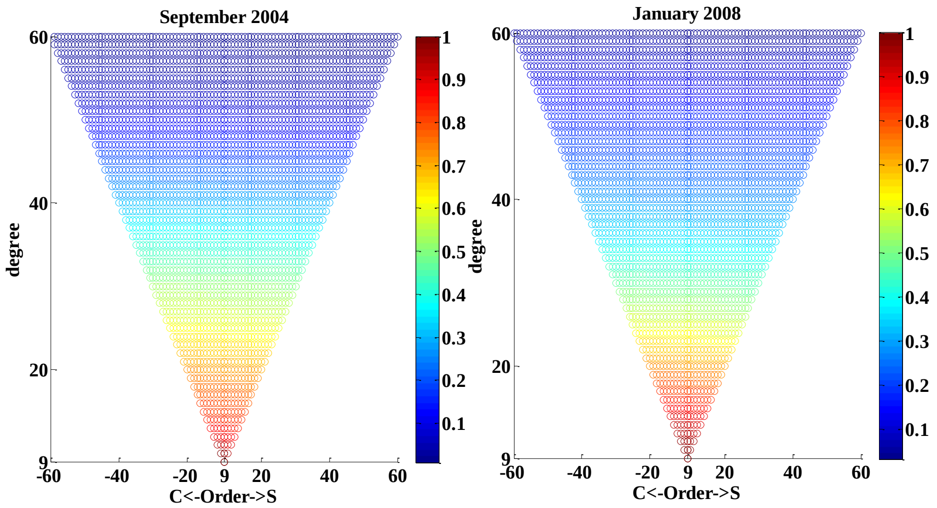

Fig. 4 The filter factors of the degree and order harmonics of September 2004 and January 2008.

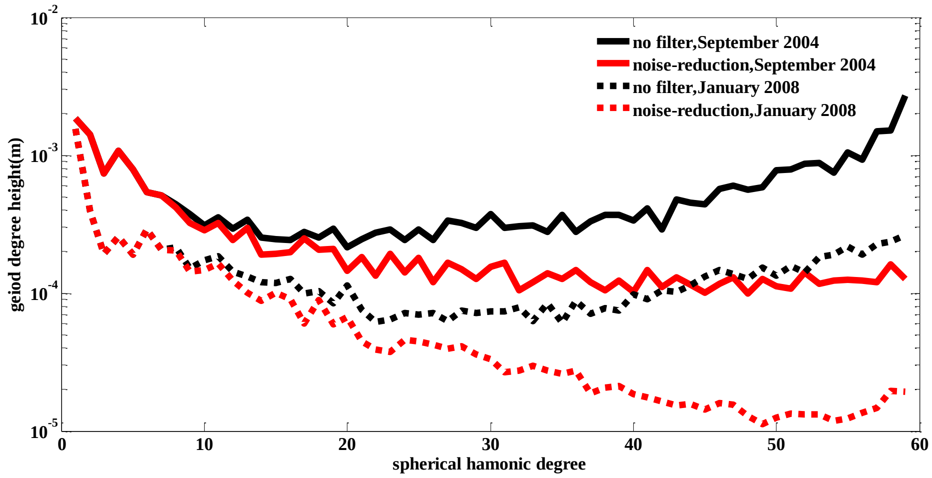

Fig. 5 The geoid degree height (log10 scale) before and after filtering.

Figure 4 presents the diagonal elements of the filter factors *F* in the form of order and degree for September 2004 and January 2008. In Figure 4 the filter factors only have slight differences for the coefficients at the same degree, but decrease fast with the increase of degrees, indicating the noise-reduction filter is like a degree-dependent, i.e., isotropic filter.

Figure 5 shows the geoid degree height for the monthly solution for September 2004 (solid line) and January 2008 (dotted line) without (black) and with the noise-reduction filter (red) applied. We can see that the geoid degree height after filtering is much smaller than that without filtering. The high degree noises are significantly suppressed, while the signals at low degrees are retained.

3. METHOD VALIDATION

The P_nM_m decorrelation filter (Swenson and Wahr, 2006; Chen et al., 2008) combined the Gaussian filter has been successfully applied in analyzing ice sheet mass balance (Chen et al., 2008; Chen et al., 2009), land-water mass changes (Wang et al., 2011), and seismic monitoring (Chen et al., 2007), also DDK filter is a successful way in the GRACE mass changes analysis (Kusche, 2007). The decorrelation filter (called PnMm) is applied to suppress the longitudinal stripes. That is, to each GRACE solution, at spherical harmonic orders *n* and above, a degree *m* polynomial is fitted by least squares and is removed from even and odd coefficient pairs. Figure 6 shows the geiod degree height for September 2004 and January 2008 after applying the P_nM_m (P_3M_8 and P_4M_6) filter and DDK1-DDK8 filters. The used GRACE data are the Tongji-Grace2018 monthly gravity solutions released on the ICGEM website. We can see that the geoid degree height from the noise-reduction filter is close to that from DDK7 for the case of September 2004 and that from DDK4 for the case of January 2008. For September 2004 and January 2008, the corresponding geoid degree height from the noise-reduction filter is both smaller than that from P_4M_6. Compared to the

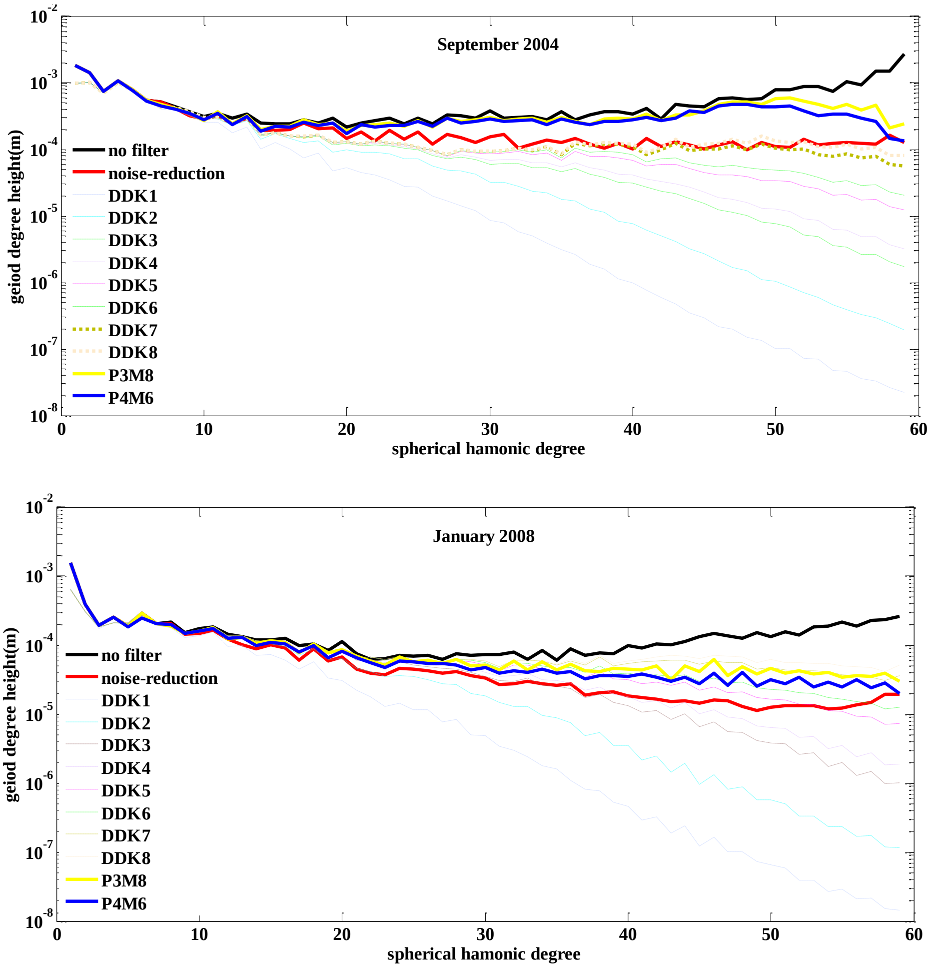

Fig. 6 The geoid degree height from noise-reduction filter, P_3M_8, P_4M_6, and DDK1-DDK8 filters.

DDK filter, the noise-reduction filter still has noise at high degrees and orders. In this case, applying an additional Gaussian filter to further suppress the remaining noise at high degrees and orders is necessary.

We choose P_nM_m (P_3M_8 and P_4M_6) filter combined with Gaussian filter and compare it to the noise-reduction filter combined with Gaussian filter. Figures 7 and 8 show the global surface mass changes based on the noise-reduction filter combined with the Gaussian filter with different radii for September 2004 and January 2008 (after subtracting the average spherical harmonic coefficients of 155 months for the time span 2002 to 2016). The radius of the Gaussian filter is selected as 0 km, 200 km and 300 km, respectively. We can find that in the case of using the same Gaussian filter radius, the striping errors of the global surface mass changes derived by applying the noise-deduced filter are significantly reduced.

The global surface mass changes derived from Tongji-GRACE2018 solution processed without any filtering and with different filtering are presented in Figures 7(d), (g), (j) and 8(d), (g), (j) for September 2004 and January 2008, respectively. In the case without any filtering, as shown in Figures 7(a) and 8(a), the north-south stripes are obvious and only limited signal can be found in some particular areas (e.g., Greenland and Antarctic Ice Sheets). We can see from Figure 7(b) (200 km Gaussian filter) and Figure 7(d) (noise-reduction filter) that the noise-reduction method suppresses much more noise as compared to the Gaussian filter. When the noise-reduction filtering or P_4M_6 or P_3M_8 decorrelation filtering is applied alone, the corresponding map of global surface mass changes is shown in Figures 7(d), 7(g) and 7(j) and 8(d), 8(g) and 8(j), where the noise still exists but it is significantly reduced as compared to that in Figures 7(a) and 8(a), especially over oceans at low latitudes. The remaining noise in Figure 7(d), especially at the medium and low latitudes is probably caused by the repeat ground track in September 2004, which leads to insufficient data sampling. As such, the unconstrained normal equation for geopotential coefficients constructed in the case of insufficient data sampling is ill-conditioned, which degrades the estimated geopotential coefficients. As a consequence, the corresponding variance-covariance matrix for the estimated geopotential coefficients, the basic for

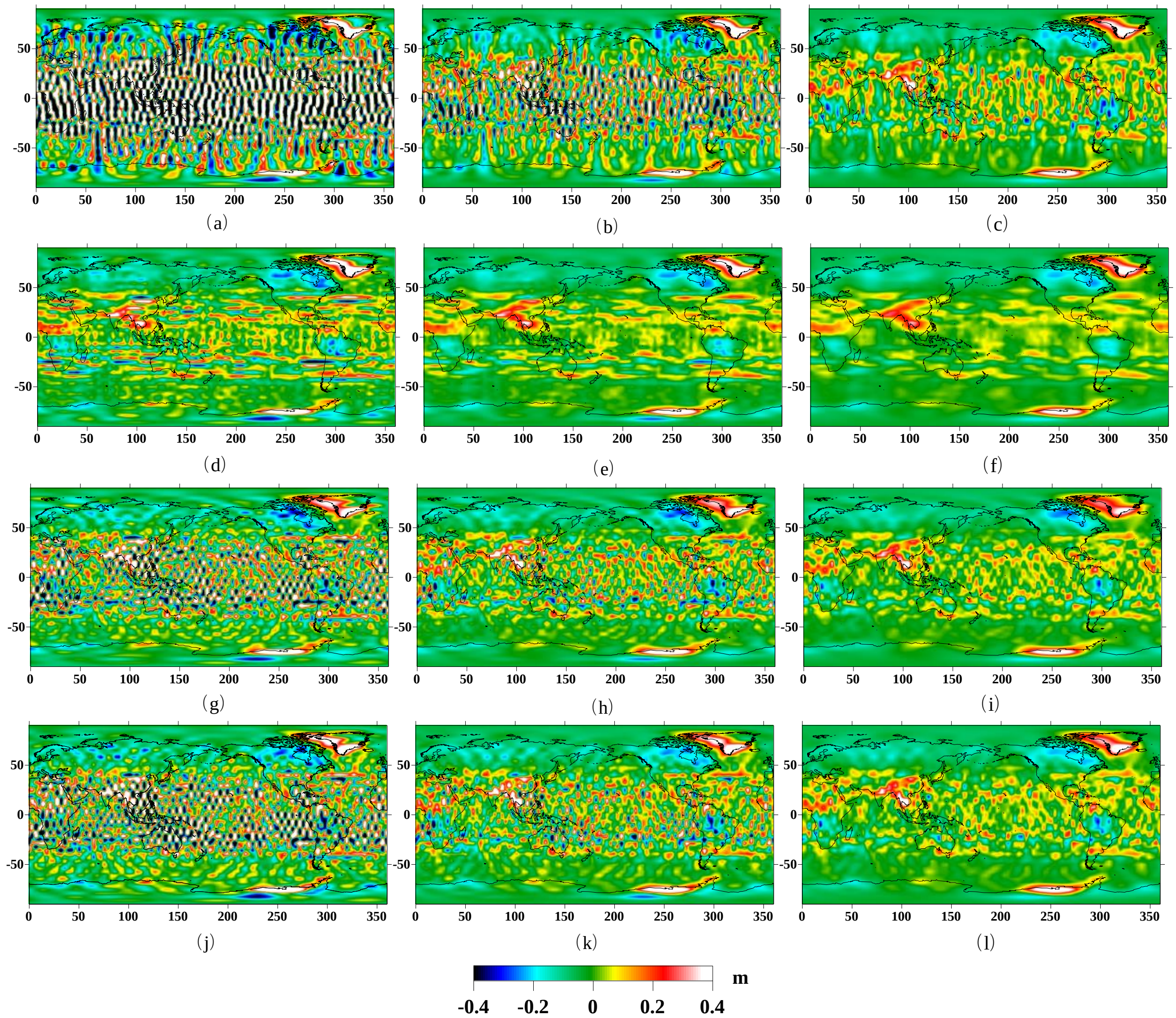

Fig. 7 The global surface mass changes in September 2004 processed by using Gaussian filter with different radii. Figures (a)(b)(c) are purely based on Gaussian filter with a radius of 0 km, 200 km, and 300 km respectively. Figures (d)(e)(f) are from the noise-reduction filter combined with the Gaussian filter with a radius of 0 km, 200 km, and 300 km separately. The sub-figures (g)(h)(i) are from a combination of P_4M_6 filter and Gaussian filter with a radius of 0 km, 200 km, and 300 km respectively. Figures (j)(k)(l) are based on the P_3M_8 filter combined with Gaussian filter with a radius of 0 km, 200 km, and 300 km respectively.

constructing our filtering matrix in this paper, lacks insufficient sampling information. Due to the insufficient sampling information at the medium and low latitudes for constructing the filtering matrix, the remaining noise can be found in September 2004 when the noise-reduction filter is applied. Nevertheless, when we compare Figure 7(d) to Figures 7(h) and 7(k), we find that the noise-reduction filter can remove the north-south stripes more effectively than P_4M_6 and P_3M_8 filters, particularly in the case of September 2004. When a Gaussian filter with a radius of 200km and 300km is individually combined with the noise-reduction filter or P_4M_6 or P_3M_8 decorrelation filter, the corresponding global surface mass changes are presented in Figures 7(e), 7(h), 7(k), 7(f), 7(i), 7(l) and 8(e), 8 (h), 8 (k), 8 (f), 8(i), 8(l), respectively, where the north-south stripes are further reduced.

The global surface mass change signals in Figure 8(e) are slightly weaker than those in Figures 8(h) and 8(k) in the Gangguo River basin located in Africa. The probable reason is the Gaussian smoothing radius used for combined filtering is determined by maximizing the signal-to-noise ratio at a global scale, which depends on the way of computing the signal-to-noise ratio. To maximize the signal-to-noise ratio at a global scale may ignore the characteristics of either signals or noise over some particular regions, which may lead to signal damping regionally. In the future, further investigations need to be conducted to discuss the way of determining the optimal Gaussian smoothing radius for combined filtering.

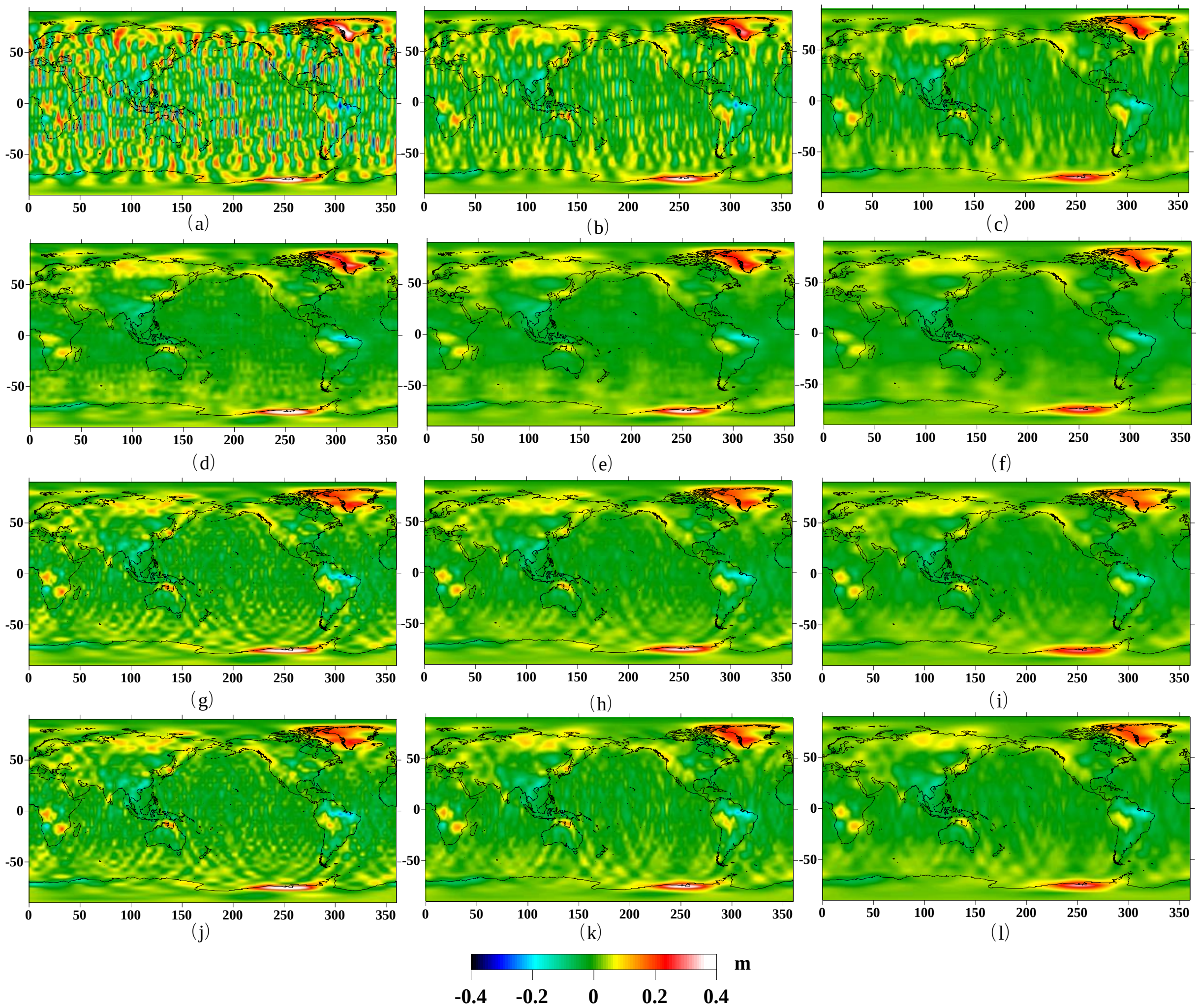

Fig. 8 Same as Figure 7, in the caption of Figure 8 but for January 2008.

4. MASS CHANGE ANALYSIS OF ANTARCTIC ICE SHEET BASED ON NOISE-REDUCTION FILTER

Based on Tongji-Grace2018 data, we analyze the mass changes over the Antarctic Ice Sheet using the noise-reduction filter and Gaussian filter compared to the combination of the P_4M_6 and P_3M_8 decorrelation and Gaussian filter. We get the signal/error ratios for AIS (The terms of trend, annual, semi-annual are composed of the signal part, while the residuals are the error part), which are 1.1376, 1.1652, 1.2009 and 1.1943 under 0 km, 100 km, 200 km and 300 km Gaussian filter radius respectively. So, the radius of 200 km is chosen. In AIS, since the low degrees have a large impact on the mass estimates (Su et al., 2020), the C_{20} coefficients are replaced by those from satellite laser ranging data (Cheng and Ries, 2017; Chen et al., 2021) and the degree-one coefficients provided in GRACE technical note 13 (TN13) (A file that provides the degree-1 coefficients (Geocenter) corrections using the GRACE-OBP method) are added back (Swenson and Wahr, 2008; Sun et al., 2016). What's more, the GIA model IJ05_R2 (Ivins et al., 2013) are applied and the leakage errors are corrected with the scale factor determined by using the GLDAS model (1.14 for Antarctica and East Antarctica, 1.2 for West Antarctica) (Loomis et al., 2020).

The time series of monthly mass changes are fitted with the terms of bias, trend and other periodical terms as follows (Földváry, 2012),

$$\begin{aligned}\Delta h(\theta,\lambda,t) = {} & \beta_0(\theta,\lambda) + \beta_1(\theta,\lambda)(t-t_0) + \beta_2(\theta,\lambda)\cos(2\pi(t-t_0)+\varphi_1(\theta,\lambda)) + \\ & + \beta_3(\theta,\lambda)\cos(4\pi(t-t_0)+\varphi_2(\theta,\lambda)) + \beta_4(\theta,\lambda)\cos(4.5342\pi(t-t_0)+\varphi_3(\theta,\lambda))\end{aligned} \tag{7}$$

where, β_0, β_1, β_2, β_3, β_4, φ_1, φ_2, φ_3 are the parameters to be solved, β_1 denotes the change rate, β_2, β_3 and β_4 are the annual, semi-annual and 161-day term respectively, φ_1, φ_2 and φ_3 are the initial phases, t is the epoch of time series in a unit of year and t_0 is the referenced epoch.

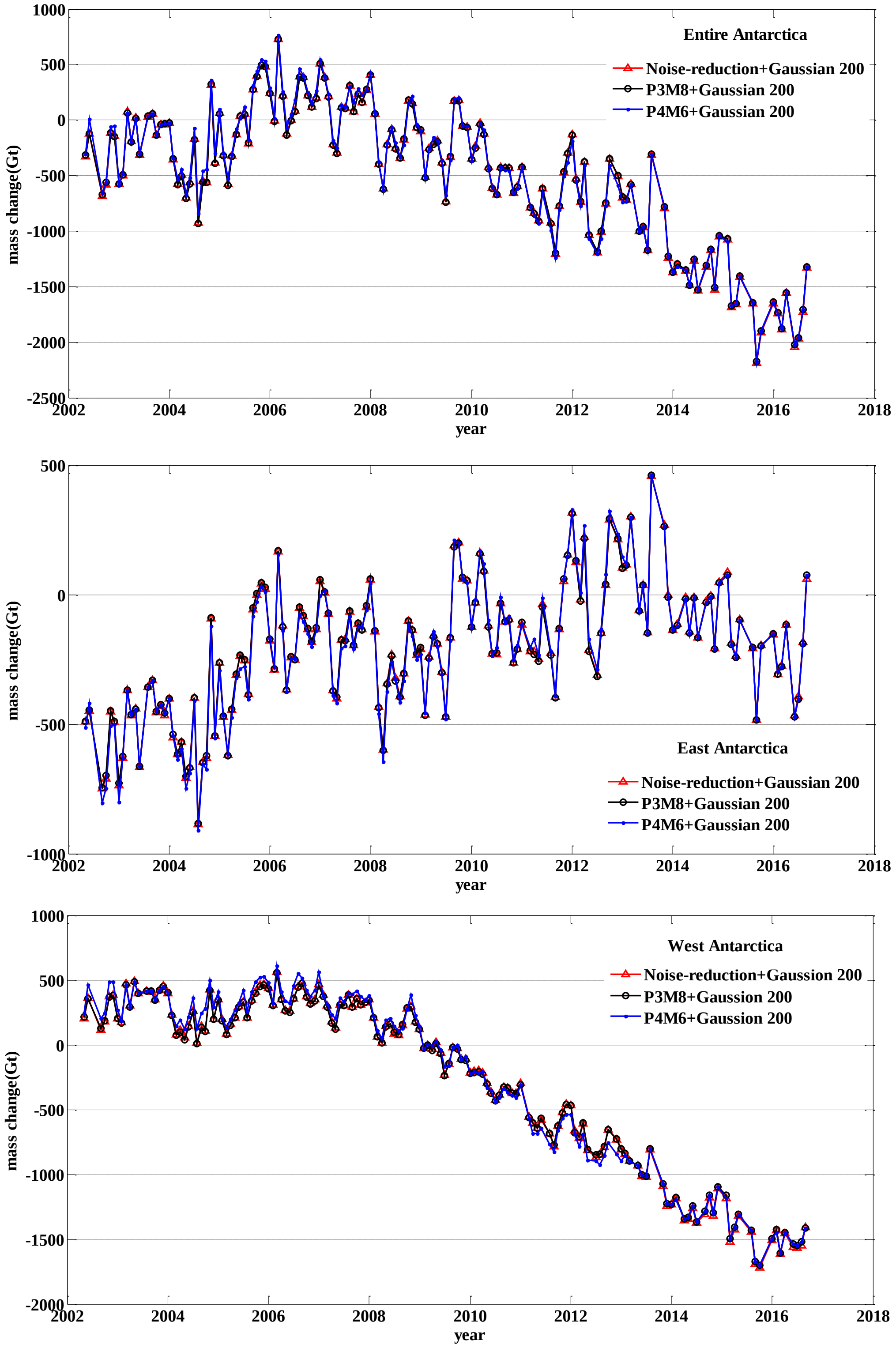

Fig. 9 The mass changes over the Entire, East and West Antarctica.

Table 1 The Antarctic ice surface mass change by different filter methods.

Methods (+Gaussian 200km)	**Entire AIS**(Gt/yr)	**East AIS**(Gt/yr)	**West AIS**(Gt/yr)
Noise-reduction filter	-107.38±41.06	36.42±14.40	-147.45± 16.78
P_3M_8 filter	-106.50±41.04	35.90±14.39	-142.41±16.75
P_4M_6 filter	-111.55±41.05	38.35±14.44	-149.90±16.78

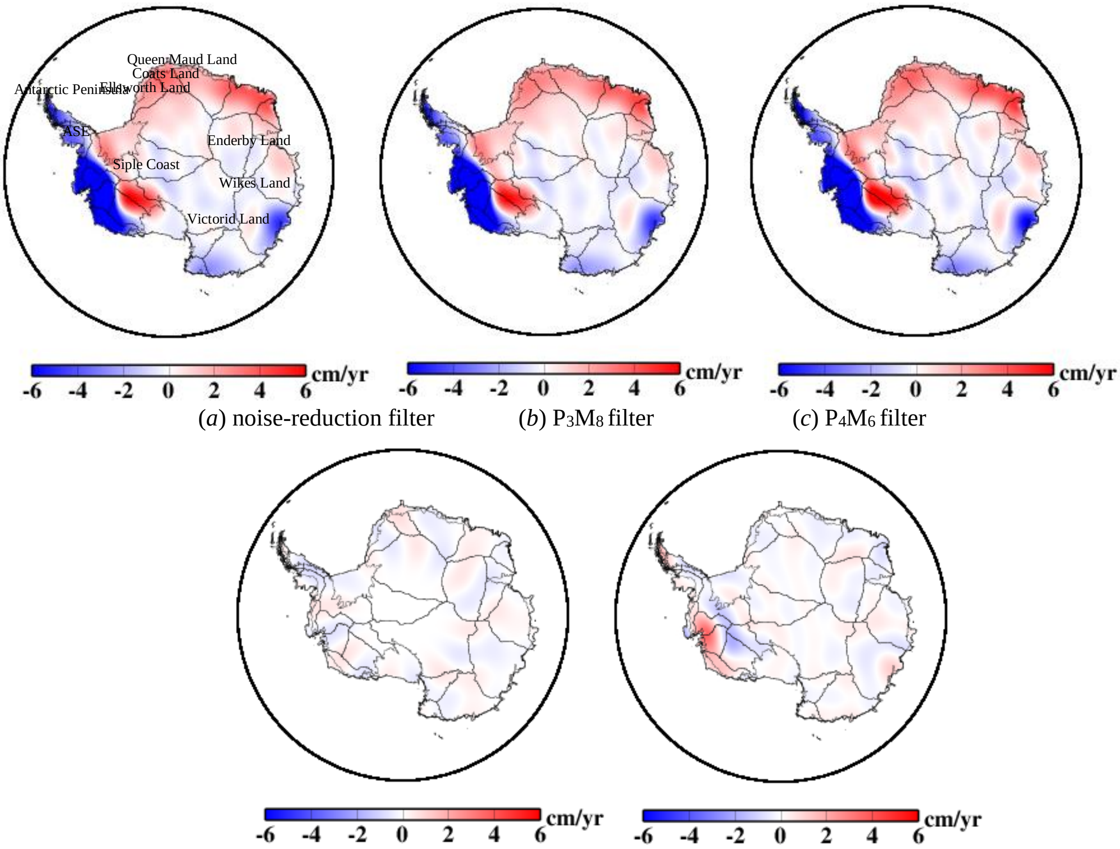

(*a*) noise-reduction filter (*b*) P_3M_8 filter (*c*) P_4M_6 filter

(d) differences between (a) and (b) (*e*) differences between (a) and (c)

Fig. 10 The trend of mass changes over Antarctica.

Figure 9 shows the time series of monthly mean surface mass changes of Entire Antarctica, East Antarctica, and West Antarctica (including the Antarctic Peninsula throughout this paper) after applying the noise-reduction filter. The uncertainty of mass change includes three parts: one is the fitting error (68.3% confidence interval) in the least-squares solution of Eq. (7), and the other two parts are the GIA model error given by Velicogna and Wahr (2013) and leakage error (Ivins et al., 2013) which are about 35 Gt/yr and 2 Gt/yr respectively. Using the Tongji-GRACE2018 data, the mass changes over the entire Antarctica and West Antarctica show an obvious decline trend, while over the East Antarctica the mass change is increasing. The mass change rates over the entire, East and West Antarctica are given in Table 1 together with the estimated uncertainties. Over the Entire Antarctica, the mass change rate is -107.38±41.06 Gt/yr, which is close to that from the P_3M_8 filter (-106.50±41.04 Gt/yr) and P_4M_6 filter (-111.55±41.05 Gt/yr). Over the East Antarctica, the mass changes increase with a trend of 36.42±14.40 Gt/yr (noise-reduction filter), 35.90±14.39 Gt/yr (P_3M_8 filter), and 38.35±14.44 Gt/yr (P_4M_6 filter). In the case of West Antarctica, the mass change trend is estimated to be - 147.45±16.78 Gt/yr for the noise-reduction filter, - 146.00±16.75 Gt/yr for the P_3M_8 filter, and - 153.73±16.78 Gt/yr for the P_4M_6 filter. In general, the results from different filtering methods are consistent within their uncertainties.

The spatial distribution of mass change rates is demonstrated in Figure 10 in the form of equivalent water height. The mass change increase mainly locates in the East Antarctica, including Coats Land (CL), Queen Maud Land (QML), Enderby Land (EL), and the Siple Coast (SC), while the main mass loss occurs in the Amundsen Sea Embayment (ASE) and Antarctic Peninsula (AP). The mass loss over the entire Antarctica is mainly contributed by the West Antarctica. Figures 10(d) and 10(e) show the difference between the mass change trends derived from the noise-reduction filter and the decorrelation filter. We can see there are slight differences (mainly between -0.4 cm/yr to 0.4 cm/yr) occurring in coastal regions, such as the QML, the Wilkes Land, Victorid Land in EA and ASE in WA, but for the inland regions, less difference can be found.

5. DISCUSSION

In Section 2, we propose the noise-reduction method. While in the processing of building the filter factor, for each solution of spherical harmonic coefficients, the filter factor corresponding to the first eigenvalue is equal to 1. In a mathematic sense, the filter factors should vary in different monthly

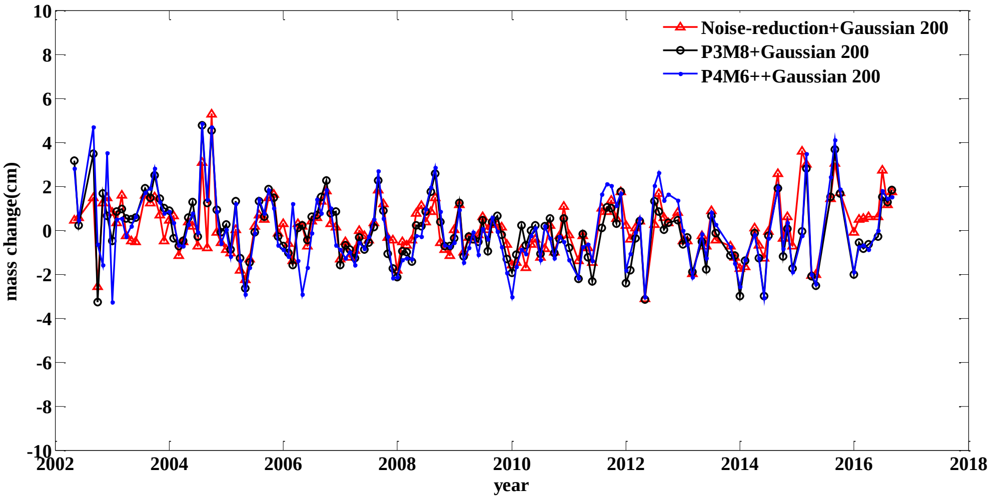

Fig. 11 The trends of mass changes over Sahara.

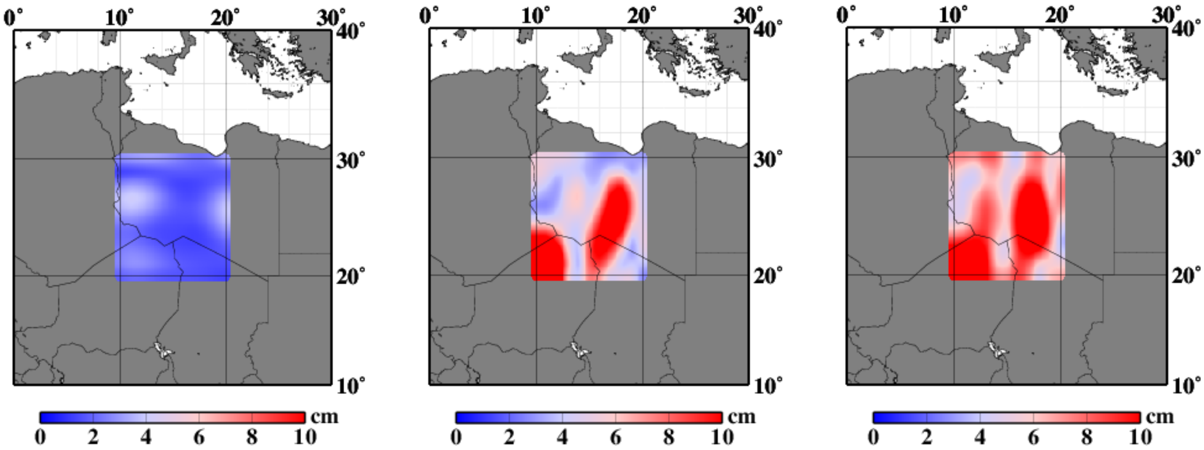

(*a*) noise-reduction filter (*b*) P_3M_8 filter (*c*) P_4M_6 filter

Fig. 12 The RMS distribution maps of Sahara.

solutions. For the high-quality monthly solution, the value should be 1, while for the worse one the value is better smaller than 1. Theoretically, the worse solution should be filtered stronger if a reasonable value can be determined to replace the first eigenvalues for the corresponding month. In general, further investigations need to be done to determine the optimal first eigenvalues for each month on the basic of careful analysis in the future.

The mass changes over Antarctica are analyzed based on the three filter methods in Section 4. Since the error of mass changes over Antarctica are smoothing to a great extent due to the large area of Antarctica, we further analyze the mass changes over Sahara Desert with weaker signals. The mass change and RMS distribution maps of Sahara desert area are shown in Figures 11 and 12 respectively. We can see from Figure 11 that the noise-reduction filter achieves the least mass changes over the Sahara among the three filtering methods. The noise-reduction filter also has the smallest mean RMS value, which is 2.13 cm, and the remaining two methods are 6.58 cm (P_3M_8 filter combined with 200 km Gaussian filter) and 7.94 cm (P_4M_6 filter combined with 200 km Gaussian filter). When we get the signal-to-error ratio, the values are 0.80 (noise-reduction filter combined with 200 km Gaussian filter), 0.45 (P_3M_8 filter combined with 200 km Gaussian filter) and 0.45 (P_4M_6 filter combined with 200 km Gaussian filter) respectively. This finding supports that the noise-reduction filter can achieve higher signal-to-noise ratio in an area with weaker signal.

6. CONCLUSIONS

In this paper, a noise-reduction filter is proposed to suppress the north-south stripes based on the error covariance matrix information of the GRACE SH solutions. The efficiency of the proposed filter is obvious during the mass change analysis over AIS and Sahara. The main conclusions can be summarized as follows:

1. Using the full error covariance matrix information of the GRACE SH coefficients, we construct the noise-reduction filter, which can suppress the noise of gravity field solutions at high degrees and effectively reduce the north-south stripes.
2. The noise-reduction filter is compared to the P_3M_8 and P_4M_6 decorrelation filters in terms of degree geoid height of GRACE SH coefficients. The results show that the degree geoid height from the noise-reduction filter is smaller than that from both P_3M_8 and P_4M_6.

Based on the combination of noise-reduction filter and Gaussian smoothing with a radius of 200 km, the mass changes over the Antarctic Ice Sheet, East and West Antarctica are analyzed. The mass change trend is estimated to be -107.38±41.06 Gt/yr over the Entire Antarctica, 36.43±14.40 Gt/yr over the East Antarctica and -147.45±16.78 Gt/yr over the West Antarctica.

AUTHOR CONTRIBUTIONS

Y.S. conceived and designed the experiments; X.J. and Q.C. performed the experiments; X.J. analyzed the data; X.J. wrote the paper; Y.S. revised the manuscript.

FUNDING

This research was funded by the Natural Science Foundation of Shandong Province (ZR201702210134; ZR2019QD003) and Shandong Jiaotong University Research Fund (Z202113).

ACKNOWLEDGMENTS

We thank ISDC for providing GRACE data.

REFERENCES

Bettadpur, S.: 2012, Insights into the Earth system mass variability from CSR-RL05 GRACE gravity fields. Geophys. Res. Abstr., 14, EGU2012-6409.

Chambers, D.P.: 2006, Evaluation of new GRACE time-variable gravity data over the ocean. Geophys. Res. Lett., 33, 17, L17603. DOI: 10.1029/2006GL027296

Chen, J.L., Ries, J.C. and Tapley, B.D.: 2021, Assessment of degree-2 order-1 gravitational changes from GRACE and GRACE Follow-on, Earth rotation, satellite laser ranging and models. J. Geod., 95, 4, 38. DOI: 10.1007/s00190-021-01492-x

Chen, Q.J., Shen, Y.Z., Chen, W., Francis, O., Zhang, X.F., Chen, Q., Li, W.W. and Chen, T.Y.: 2019, An optimized short-arc approach: Methodology and application to develop refined time series of Tongji-Grace2018 GRACE monthly solutions. J. Geophys. Res., Solid Earth, 124, 6, 6010–6038. DOI: 10.1029/2018JB016596

Chen, J.L., Wilson, C.R., Blankenship, D. and Tapley, B.D.: 2009, Accelerated Antarctic ice loss from satellite gravity measurements. Nat. Geosci., 2, 12, 859–862. DOI: 10.1038/ngeo694

Chen, J.L., Wilson, C.R. and Seo, K.W.: 2006, Optimized smoothing of gravity recovery and climate experiment (GRACE) time variable gravity observations. J. Geophys. Res., Solid Earth., 111, B06408. DOI: 10.1029/2005JB004064

Chen, J.L., Wilson, C.R., Tapley, B.D., Blankenship, D. and Young, D.: 2008, Antarctic regional ice loss rates from GRACE. Earth Planet. Sci. Lett., 266, 1, 140–148. DOI: 10.1016/j.epsl.2007.10.057

Chen, J.L., Wilson, C.R., Tapley, B.D. and Grand, S.: 2007, GRACE detects coseismic and postseismic deformation from the Sumatra-Andaman earthquake. Geophys. Res. Lett., 34, 13, 173–180. DOI: 10.1029/2007GL030356

Cheng, M.K. and Ries, J.C.: 2017, The unexpected signal in GRACE estimates of C20. J. Geod., 91, 897–914. DOI: 10.1007/s00190-016-0995-5

Davis, J.L., Tamisiea, M.E., Elósegui,P., Mitrovica, J.X. and Hill, E.M.: 2008, A statistical filtering approach for Gravity Recovery and Climate Experiment (GRACE) gravity data. J. Geophys. Res., Solid Earth, 113, B04410. DOI: 10.1029/2007JB005043

Duan, X.J., Guo, J.Y., Shum, C.K. and van der Wal, W.: 2008, On the postprocessing removal of correlated errors in GRACE temporal gravity field solutions. J. Geod., 83, 11,1095–1106. DOI: 10.1007/s00190-009-0327-0

Fengler, M.J., Freeden, W., Kohlhaas, A., Michel, V. and Peters, T.: 2007, Wavelet modeling of regional and temporal variations of the earth's gravitational potential observed by GRACE. J. Geod., 81, 1, 5–15. DOI: 10.1007/s00190-006-0040-1

Földváry, L.: 2012, Mass-Change Acceleration in Antarctica from GRACE Monthly Gravity Field Solutions. IAG Symposia, 136, 3, 591–596. DOI: 10.1007/978-3-642-20338-1_72

Gao, C.C., Lu, Y., Shi, H.L., Zhang, Z.Z., Xu, C.Y. and Tan, B.: 2019, Detection and analysis of ice sheet mass changes over 27 Antarctic drainage systems from grace RL06 data. Chin. J. Geophys., 62, 3, 864–882. DOI: 10.6038/cjg2019M0586

Guo, J.Y., Li, W.D., Chang, X.T., Zhu, G.B., Liu, X. and Guo, B.: 2018, Terrestrial water storage changes over Xinjiang extracted by combining Gaussian filter and multichannel singular spectrum analysis from GRACE. Geophys. J. Int., 213, 1, 397–407. DOI: 10.1093/gji/ggy006

Han S.-Ch., Shum, C.K., Jekeli Ch., Kuo Ch.-Y., Wilson, C. and Seo, K.-W: 2005, Non-isotropic filtering of GRACE temporal gravity for geophysical signal enhancement. Geophys. J. Int., 163, 1, 18–25. DOI: 10.1111/j.1365-246X.2005.02756.x

Ivins, E.R., James, T.S., Wahr, J., Schrama, E.J.O., Landerer, F.W. and Simon, K.M.: 2013, Antarctic contribution to sea-level rise observed by GRACE with improved GIA correction. J. Geophys. Res., 118, 6, 3126–3141. DOI: 10.1002/jgrb.50208

Jekeli, C.: 1981, Alternative methods to smooth the Earth's Gravity Field. Rep. 327, Department of Geodetic Science and Surveying, Ohio State University, Columbus, OH.

Ju, X.L., Shen, Y.Z. and Zhang, Z.Z.: 2014, GRACE RL05-based ice mass changes in the typical regions of Antarctica from 2004 to 2012. Geod. Geodyn., 5, 4, 57–67. DOI: 10.3724/SP.J.1246.2014.04057

Klees, R., Revtova, E.A., Gunter, B.C., Ditmar, P., Oudman, E. and Winsemius, H.C.: 2008, The design of an optimal filter for monthly GRACE gravity models. Geophys. J. Int., 175, 2, 417–432. DOI: 10.1111/j.1365-246X.2008.03922.x

Kusche, J.: 2007, Approximate decorrelation and non-isotropic smoothing of time-variable GRACE-type gravity field models. J. Geod., 81, 11, 733–749. DOI: 10.1007/s00190-007-0143-3

Kusche, J., Schmidt, R., Petrovic, S. and Rietbroek, R.: 2009, Decorrelated GRACE time-variable gravity solutions by GFZ, and their validation using a hydrological model. J. Geod., 83, 10, 903–913. DOI: 10.1007/s00190-009-0308-3

Loomis, B.D., Rachlin, K.E., Wiese, D.N., Landerer, F.W. and Luthcke, S.B.: 2020, Replacing GRACE/GRACE-FO C30 with satellite laser ranging: Impacts on Antarctic Ice Sheet mass change. Geophys. Res. Lett., 47, 3. DOI: 10.1029/2019GL085488

Panet, I., Mikhailov, V.O., Diament, M. et al.: 2007, Coseismic and post-seismic signatures of the Sumatra 2004 December and 2005 March earthquakes in GRACE satellite gravity. Geophys. J. Int., 171, 1, 177–190. DOI: 10.1111/j.1365-246X.2007.03525.x

Prevost, P., Chanard, K., Fleitout, L., Calais, E., Walwer, D., Van Dam, T. and Ghill, M.: 2019, Data-adaptive spatio-temporal filtering of GRACE data. Geophys. J. Int., 219, 2034–2055. DOI: 10.1093/gji/ggz409

Rangelova, E., van der Wal, W., Braun, A., Sideris, M. G. and Wu, P.: Analysis of Gravity Recovery and Climate Experiment time-variable mass redistribution signals over North America by means of principal component analysis. J. Geophys. Res., Earth Surface, 112, F3. DOI: 10.1029/2006JF000615

Sasgen, I., Martinec, Z. and Fleming, K.: 2006, Wiener optimal filtering of GRACE data. Stud. Geophys. Geod., 50, 4, 499–508. DOI: 10.1007/s11200-006-0031-y

Shepherd, A., Ivins, E.R., Geruo A., Barletta, V.R., Bentley, M.J., Bettadpur, S., Briggs, K.H., Bromwich, D.H., Forsberg, R., Galin, N., Horwath, M., Jacobs, S., Joughin, L., King, M.A., Lenaerts, J.T.M., Li, J.L., Ligtenberg, S.R.M., Luckman, A., Luthcke, S.B., McMillan, M., Meister, R., Milne, G., Mouginot, J., Muir, A., Nicolas, J.P., Paden, J., Payne, A.J., Pritchard, H., Rignot, E., Rott, H. Sorensen, L.S., Scambos, T.A., Scheuchl, B., Schrama, E.J.O., Smith, B., Sundal, A.V., van Angelen, J.H., van den Berg, W.J., van den Broeke, M.R., Vaughan, D.G., Velicogna, I., Wahr, J., Whitehouse, P.L., Wingham, D.J., Yi, D., Young, D. and Zwally, H.J.: 2012, A reconciled estimate of ice-sheet mass balance. Science., 338, 6111, 1183–1189. DOI: 10.1126/science.1228102

Shum, C.K., Kuo, C.Y. and Guo, J.Y.: 2008, Role of Antarctic ice mass balance in present-day sea-level change. Polar Sci., 2, 149–161. DOI: 10.1016/j.polar.2008.05.004

Simons, F.J., Dahlen, F.A. and Wieczorek, M.A.: 2006, Spatiospectral concentration on a sphere. SAIM Rev., 48, 3, 504–536.

Su, X.L., Guo, J.Y., Shum, C.K., Luo, Z.C. and Zhang, Y.: 2020, Increased low degree spherical harmonic influences on polar ice sheet mass change derived from GRACE Mission. Remote Sens., 12, 24, 4178. DOI: 10.3390/rs12244178

Sun,Y., Riva, R. and Ditmar, P.: 2016, Optimizing estimates of annual variations and trends in geocenter motion and J2 from a combination of GRACE data and geophysical models. J. Geophys. Res., Solid Earth, 121, 11, 8352–8370. DOI: 10.1002/2016JB013073

Swenson, S. and Wahr, J.: 2006, Post-processing removal of correlated errors in GRACE data. Geophys. Res. Lett., 33, 8. DOI: 10.1029/2005GL025285

Tapley, B.D., Bettadpur, S., Watkins, M. and Reigber, C.: 2004, The gravity recovery and climate experiment: mission overview and early results. Geophys. Res. Lett., 31, 9, L09607. DOI: 10.1029/2004GL019920

Velicogna, I., Sutterley, T.C. and Van Den Broeke, M.R.: 2014, Regional acceleration in ice mass loss from Greenland and Antarctica using GRACE time-variable gravity data. Geophys. Res. Lett., 41, 22, 8130–8137. DOI: 10.1002/2014gl061052

Velicogna, I. and Wahr, J.: 2013, Time-variable gravity observations of ice sheet mass balance: Precision and limitations of the GRACE satellite data. Geophys. Res. Lett., 40, 3055–3063. DOI: 10.1002/grl.50527

Wahr, J., Swenson, S. Zlotnicki, V. and Velicogna, I.: 2004, Time-variable gravity from GRACE: First results. Geophys. Res. Lett., 31, 11, L11501. DOI: 10.1029/2004GL019779

Wang, X., Linage, C.D., Famiglietti, J. and Zender, C.S.: 2011, Gravity Recovery and Climate Experiment (GRACE) detection of water storage changes in the Three Gorges Reservoir of China and comparison with in situ measurements. Water Resour. Res., 47, 12, W12. DOI: 10.1029/2011WR010534

Wang, F.W., Shen, Y.Z., Chen, T.Y., Chen, Q.J. and Li, W.W.: 2020, Improved multichannel singular spectrum analysis for post-processing GRACE monthly gravity field models. Geophys. J. Int., 223, 825–839. DOI: 10.1093/gji/ggaa339

Wouters, B. and Schrama, E.J.O.: 2007, Improved accuracy of GRACE gravity solutions through empirical orthogonal function filtering of spherical harmonics. Geophys. Res. Lett., 34, 23, DOI: 10.1029/2007gl032098

Zhang, Z.Z., Chao, B.F., Lu, Y. and Hsu, H.Z.: 2009, An effective filtering for GRACE time-variable gravity: Fan filter. Geophys. Res. Lett., 36, 17, L17311. DOI: 10.1029/2009GL039459

Zotov, L.V. and Shum, C.K.: 2010, Multichannel singular spectrum analysis of the gravity field data from GRACE satellites. AIP Conf. Proc., 1206, 473. DOI: 10.1063/1.3292557

Zou, F., Tenzer, R. and Rathnayake, S.: 2019, Monitoring changes of the Antarctic Ice sheet by GRACE, ICESat and GNSS. Contrib. Geophys. Geod., 49, 4, 403–424. DOI: 10.2478/congeo-2019-0021